

RESEARCH ARTICLE

View Article Online
View Journal

Cite this: DOI: 10.1039/d6qi00499g

Water splitting with cobalt-incorporated ruthenium sulfide (Co_xRuS) and a molecular cobalt porphyrin

Nasim Jafari, Neidy Ocuane, Brenda Torres, Jose L. Lasso, Carlos R. Cabrera and Dino Villagrán *

Here we present a one-step synthesis of bimetallic cobalt ruthenium sulfide on Vulcan XC-72R carbon (C-Co_xRuS) for electrochemical water splitting, which was coupled with CoTcPP (cobalt 5,10,15,20-tetrakis(4-carboxyphenyl) porphyrin) for improved Oxygen Evolution Reaction (OER) electrocatalysis. Electrochemical analyses reveal that increasing cobalt content enhances the maximum current density by 8x for HER and 3x for OER. The optimized C-Co₄RuS catalyst demonstrates bifunctional activity with an HER overpotential of -75 mV (vs. RHE) at 10 mA cm⁻² and a Tafel slope of 75 mV dec⁻¹ for HER (Volmer–Heyrovsky mechanism) and an overpotential of 257 mV (vs. RHE) at 10 mA cm⁻², with a Tafel slope of 95 mV dec⁻¹ for OER. The addition of cobalt to the ruthenium sulfide material facilitates charge transfer and improves active site accessibility according to Electrochemical Impedance Spectroscopy (EIS) and Electrochemical Active Surface Area (ECSA) results. Upon CoTcPP compositing the OER overpotential and Tafel slope decrease to 202 mV (vs. RHE) and 79 mV dec⁻¹ respectively, further improving its catalytic activity. These results show that C-Co_xRuS/CoTcPP can be an efficient, bifunctional electrocatalyst, providing a viable alternative to common electrocatalysts for water splitting in sustainable energy applications.

Received 13th March 2026.
Accepted 8th May 2026

DOI: 10.1039/d6qi00499g

rsc.li/frontiers-inorganic

Introduction

Hydrogen, with a high energy density (146 kJ g⁻¹) and zero carbon emissions, has emerged as a sustainable solution to the growing problems of energy depletion and environmental contamination.^{1,2} Currently, the primary method for producing hydrogen on a large scale is through the steam reforming of methane.³ This process requires high temperature and releases significant amounts of carbon dioxide.⁴ Therefore, developing efficient and environmentally sustainable hydrogen production methods is crucial.⁵ Among various alternatives, water splitting into hydrogen and oxygen through electrolysis presents a promising approach to avoid these issues.⁶

Water splitting consists of two half-reactions: the hydrogen evolution reaction (HER) and the oxygen evolution reaction (OER). While HER directly produces hydrogen, OER plays a crucial role in completing the overall redox cycle.^{7,8} HER and OER occur at 0 V and 1.23 V *versus* the reversible hydrogen electrode (RHE) at 298 K, respectively.⁹ However, additional energy is often required to overcome the activation energy to initiate the reaction.¹⁰ A key limitation in this process is the sluggish kinetics of the OER, the four-electron half reaction that signifi-

cantly limits overall water splitting efficiency.^{11–13} To address this bottleneck, the development of efficient electrocatalysts is critical. Electrocatalysts reduce the overpotential, enhance reaction kinetics, and improve energy conversion efficiency.⁷ In designing such catalysts, factors like activity, stability, cost, and ease of synthesis must be considered.¹⁴ Platinum-based materials are widely regarded as benchmark HER catalysts due to their performance.^{15–18} However, the high cost and scarcity of platinum hinder its widespread application.¹⁹

Transition metal chalcogenides (TMCs), particularly sulfides, have gained interest for electrocatalysis due to their good electrical conductivity and variable oxidation states, which in turn, enhance redox activity.^{20–23} Like the hydrogenase enzyme structure, the high activity of transition metal sulfides for hydrogen production is likely due to the presence of metal sulfur clusters with five ligands that are arranged in a distorted octahedral configuration.^{24–26} Ruthenium disulfide (RuS₂) is a transition metal sulfide that is known for its catalytic activity in hydrodesulfurization (HDS).²⁷ Numerous studies have shown that catalysts effective for HDS also excel as HER electrocatalysts, as both reactions involve reversible hydrogen binding to the catalyst.^{24,28} While ruthenium is classified as a precious metal, it is significantly more affordable than platinum, so ruthenium-based materials have gained attention as lower-cost alternatives for platinum in HER.²⁹ Recent studies have demonstrated that Ru-based nano-

Department of Chemistry and Biochemistry, The University of Texas at El Paso, El Paso, Texas, 79968, USA. E-mail: dino@utep.edu

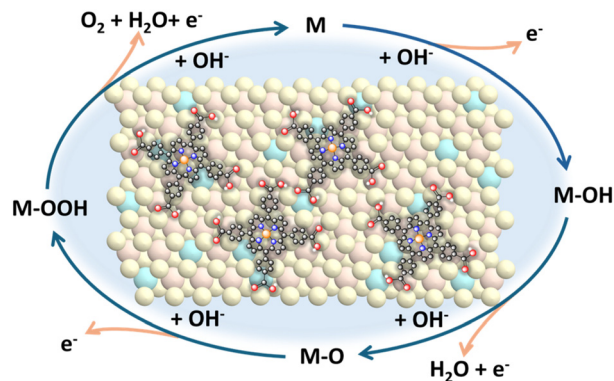


structures, heterostructures, and hybrid catalysts can deliver excellent hydrogen-evolution activity through optimized hydrogen adsorption energetics, improved conductivity, and reduced noble-metal loading. Representative examples include Ru-containing composite catalysts, defect-engineered Ru systems, and interfacial Ru-based electrocatalysts reported in recent literature.^{30–32} Although RuS₂ has shown promise for HER-related electrocatalysis, its broader application in water splitting, particularly under anodic OER conditions, remains comparatively underexplored. Additionally, high ruthenium loadings are often required, which raises cost concerns and compromises stability under OER conditions due to the susceptibility of ruthenium to oxidation at high potentials.³³

To improve both the activity and stability of ruthenium-based catalysts, recent efforts have focused on compositional tuning.³⁴ Introducing a second transition metal, such as cobalt, into sulfide systems has been shown to enhance electrochemical performance through electronic modulation, broader accessible oxidation states, and narrowed band gaps compared with single-metal sulfides.^{35,36} For example, cobalt ruthenium sulfide electrodes have shown promising electrochemical activities as supercapacitors, which suggests its potential for electrocatalysis.³⁷

Another promising approach is incorporating porphyrin-based molecular structures.^{38,39} Porphyrins are a group of highly conjugated macrocyclic compounds known for their structural versatility, chemical tunability, and stable π -conjugated systems.⁴⁰ The electronic and chemical properties of porphyrins can be precisely adjusted through metalation, peripheral functionalization, and substitution at the *meso* or β -positions, which in turn allow for control over redox behavior and molecular interactions.⁴¹ As a result, porphyrins have gained attention in energy conversion applications, particularly in electrocatalysis and photoelectrocatalysis.⁴² In water splitting, metalloporphyrins, such as cobalt, nickel, and iron porphyrins, have shown notable activity in OER, due to their ability to support multi-electron transfer and stabilize reactive intermediates.^{43–45} Recent work has further shown that porphyrin-based metal architectures, particularly cobalt-centered systems, can promote oxygen electrocatalysis by providing structurally defined active sites and facilitating multi-electron O–O bond-forming pathways, showing the broader value of tunable porphyrin motifs in water-splitting catalyst design.^{46–48} Coupling these modified molecular frameworks with ruthenium sulfide can provide tunable structures and efficient electron transfer pathways that can stabilize active sites,³⁸ while reducing the required ruthenium content.

Herein, we report a modified one-step synthesis method for cobalt ruthenium sulfide supported on carbon (C-Co_xRuS) as a HER/OER catalyst and its composite with cobalt porphyrin (CoTcPP) as a catalyst for OER in electrochemical water splitting (Scheme 1). The introduction of cobalt into the ruthenium sulfide matrix enhanced catalytic performance while reducing the overall ruthenium content. Furthermore, with the addition of CoTcPP, the resulting composite exhibits a significantly lower OER overpotential and faster kinetics, evidenced by a



Scheme 1 Schematic illustration of oxygen evolution reaction (OER) on CoTcPP/C-Co₄RuS catalytic surface (M represents metal active sites of Co and Ru).

smaller Tafel slope, than its constituent components. These improvements may arise from electronic interactions between the mixed-valence cobalt and ruthenium centers, which facilitate more efficient redox reactions, and the cobalt porphyrin, whose conjugated molecular structure promotes electron delocalization and enhances charge transfer. Together, these features increase the accessibility and utilization of active sites, resulting in improved electrocatalytic performance.

Experimental

Materials

Ruthenium chloride hydrate (RuCl₃·xH₂O), cobalt nitrate hexahydrate (Co(NO₃)₂·6H₂O), 4-carboxybenzaldehyde, propionic acid, and pyrrole were purchased from Sigma-Aldrich. Vulcan XC-72R carbon black powder was ordered from CABOT. Nafion was purchased from Alfa Aesar. All the chemicals were used as received without further purification.

Synthesis of C-Co_xRuS

C-Co_xRuS ($x = \text{Co/Ru molar ratio} = 0, 1, 2, \text{ and } 4$) samples were synthesized through a modified one-step method. For C-CoRuS, C-Co₂RuS, and C-Co₄RuS, 178 mg, 118 mg, and 71 mg RuCl₃·xH₂O and 250 mg, 333 mg, and 400 mg Co(NO₃)₂·6H₂O were used, respectively. For C-RuS, 270 mg RuCl₃·xH₂O was used. 0.5 ml DI water was added to each mixture and mixed with 200 mg Vulcan carbon. The resulting thick paste was placed in a Porcelain combustion boat and placed inside a tubular furnace. At a temperature of 300 °C, a gaseous flow of 15% H₂S/H₂ was passed through the furnace with a flow rate of 400 ml min⁻¹ for 3 hours. Then the furnace was cooled down, and the resulting black powders were collected for characterization.

Synthesis of cobalt 5,10,15,20-tetrakis(4-carboxyphenyl) porphyrin (CoTcPP)

CoTcPP was synthesized according to the previously reported procedure.³⁸ 5 g of 4-carboxybenzaldehyde (33.3 mmol) was



dissolved in 500 mL of propionic acid and heated to 140 °C until complete dissolution. Then 2.23 g pyrrole (33.3 mmol) was added dropwise to the mixture, which was then refluxed under constant stirring for 2 hours. Then, 100 mL MeOH was added to the reaction, and the mixture was cooled down using an ice bath. The product was filtered using a medium-coarse filter frit. The solid product (H₂TcPP) was then washed with deionized water and dried under vacuum to obtain a dark purple powder. Afterward, 0.1 g H₂TcPP (0.126 mmol) and 0.0266 g anhydrous Co(OAc)₂ (0.15 mmol) were dissolved in 20 mL of DMF and were refluxed for one hour. After allowing the reaction mixture to cool, the resulting product was filtered, and the filtrate was washed with DI water and dried under vacuum at 80 °C. The resulting purple powder (0.089 g) with a yield of 83% was characterized by the UV-Vis technique. The UV-Vis spectrum of CoTcPP in DMF displays a pronounced Soret band around 430 nm and distinct Q bands of 550 nm and 595 nm (Fig. S1), confirming the successful synthesis of CoTcPP.

Also, the CoTcPP/C-Co₄RuS used in this study was prepared through a physical mixture of 10 wt% CoTcPP with the C-Co₄RuS catalyst. The purpose of this combination was to investigate the functional synergy between the molecular Co-porphyrin species (which facilitate O–O bond formation *via* Co–N₄ centers) and the conductive C-Co_xRuS framework.

Characterization methods

The phase identification through powder X-ray diffraction (pXRD) was conducted by a Panalytical Empyrean 2 X-ray diffractometer system, using Cu-K α radiation ($\lambda = 1.5416 \text{ \AA}$) in 2 θ range of 5–90 and 10-minute scans. The morphology analysis and microscopic surface image of the samples were collected using a Hitachi S4800 scanning electron microscope (SEM) coupled with a Bruker EDX XFlash 6I60 energy-dispersive spectroscopy (EDS) system for elemental mapping. For this, the powdered sample was stuck on an aluminum stub using conductive carbon tape. Furthermore, transmission electron microscopy (TEM) imaging was conducted by a JEM-3200FS field emission electron microscope equipped with a field emission electron gun operating at an accelerating voltage of 300 kV, while the samples were drop-cast onto copper grids. X-ray photoelectron spectroscopy spectra (XPS) were collected on a XPS Nexsa G2 instrument for analysing the chemical composition and oxidation states of the samples. The XPS analysis was done with an Al K α monochromatic source, with a pass energy of 50.0 eV. The binding energies were referenced to C 1s at 285.0 eV.

Electrochemical measurements

Electrochemical measurements were carried out with a CH Instrument potentiostat (760E) at room temperature in a three-electrode cell. A graphite rod was used as the counter electrode for both HER and OER experiments. For HER, the electrolyte was 0.5 M H₂SO₄ aqueous solution, and the reference electrode was saturated calomel electrode (SCE), while for OER experiments the electrolyte was 1.0 M KOH aqueous solution, and a

Hg/HgO (1.0 M NaOH) alkaline reference electrode. The working electrode was carbon paper coated with a drop-casted catalyst ink. The ink was made by a homogenous mixture of 5 mg of the electrocatalyst, 2.5 mg of carbon black, 5.0 μl of Nafion as a binding agent, and 1.0 ml of isopropyl alcohol. The solution was sonicated for 15 minutes to make a homogeneous solution and was pipetted on the carbon paper with a loading of 20 μl in a 1.0 \times 1.0 cm² area. The ink was allowed to dry at room temperature for one hour to leave a uniform layer of material with a catalyst loading of 0.1 mg cm⁻².

Linear Sweep Voltammetry (LSV) was done at a scan rate of 5 mV s⁻¹ after correcting with *iR* compensation, and the potential was reported *versus* the reversible hydrogen electrode (RHE) through the following equations:

$$E_{\text{RHE}} = E_{\text{SCE}} + 0.2415 + 0.0591 \times \text{pH} \quad (1)$$

$$E_{\text{RHE}} = E_{\text{Alkaline}} + 0.098 + 0.0591 \times \text{pH} \quad (2)$$

with a pH of 0 for HER experiments and 14 for OER.

The performance of these materials was analyzed through Tafel plots by using the stepped potentiostatic method, in which the potential change was conducted stepwise with a 30 s holding time at each potential to avoid capacitive current interruption. Then the equation $\eta = b \log j + a$ was applied, which describes the relationship between overpotential (η) and current density (j), where b represents the Tafel slope and a is a constant.⁴⁹ The slope of the linear region of the resulting plot is recorded as the Tafel.

Electrochemical Impedance Spectroscopy (EIS) measurements were done with a frequency range of 0.1 Hz to 100 kHz at a potential of 0.2 V at room temperature in a 4 mM solution of Fe(CN)₃^{-/4-} in 0.1 M KCl.

The electrochemical active surface area (ECSA) was estimated using cyclic voltammetry (CV) in a non-faradaic region at varying scan rates to determine the electrochemical double-layer capacitance (C_{dl}). From these CVs, the capacitive current at each scan rate is plotted, and the slope of the linear fit yields C_{dl} . Then, ECSA is calculated by dividing by the specific capacitance (C_s) for the catalyst material.⁵⁰

All voltammograms in this work are presented following the U.S. (polarographic) convention, where cathodic (reductive) currents are plotted as positive and anodic (oxidative) currents as negative. The potential axis is displayed with more negative potentials toward the right and more positive potentials toward the left. This convention was used consistently throughout all figures for clarity and uniformity.⁵¹

Results and discussion

Characterization

Cobalt and ruthenium sulfide have been synthesized through various methods, including hydrothermal, solvothermal, colloidal, and gas-phase sulfidation techniques.^{37,52–54} Among these, gas-phase sulfidation, where metal precursors are supported on a conductive substrate and converted under H₂S/H₂



flow, offers good control over phase formation and dispersion.⁵⁵ In this study, we employed a modified version of this method using a solvent-limited paste composed of cobalt and ruthenium salts with Vulcan carbon. This approach minimized solvent use, enhanced precursor dispersion, and improved contact with the support, leading to more uniform sulfidation and improved electrochemical performance. The effectiveness of this synthesis method is reflected in the structural characterization of the resulting materials. Fig. 1 presents the powder X-ray diffraction (PXRD) patterns of C-Co₄RuS, C-Co₂RuS, and C-CoRuS samples compared with the standard XRD patterns of RuS₂ (JCPDS No. 04-003-3003, indicated by red squares) and Co₉S₈ (JCPDS No. 04-006-5681, marked by blue asterisks). The diffraction peaks in Fig. 1, at 2θ of 27.7°, 31.9°, 36.1°, 45.8°, and 54.3°, can be ascribed as (111), (200), (210), (220), (311) planes of cubic pyrite-RuS₂ (JCPDS No. 04-003-3003)³³ and 15.4°, 29.8°, 31.1°, 39.5°, 47.5° and 52° can be ascribed as (111), (311), (222), (331), (511), (440) planes of Co₉S₈ (JCPDS No. 04-006-5681).⁵⁶ All synthesized samples show characteristic peaks corresponding to both RuS₂ and Co₉S₈ phases, confirming the successful formation of a bimetallic sulfide structure. As the cobalt content increases from C-CoRuS to C-Co₄RuS, the intensity of the Co₉S₈ peaks becomes more pronounced, indicating a higher degree of cobalt in the composite. Also, the presence of sharp and well-defined peaks in all samples suggests a good crystallinity.

The morphology of C-Co₄RuS was investigated through Scanning Electron Microscopy (SEM) and Transmission Electron Microscopy (TEM) techniques. The SEM image in Fig. 2a consists of polyhedral particles with sizes around 0.5–1 μm, while the TEM image in Fig. 2b shows that these structures are composed of interconnected nanosized particles (5–20 nm).

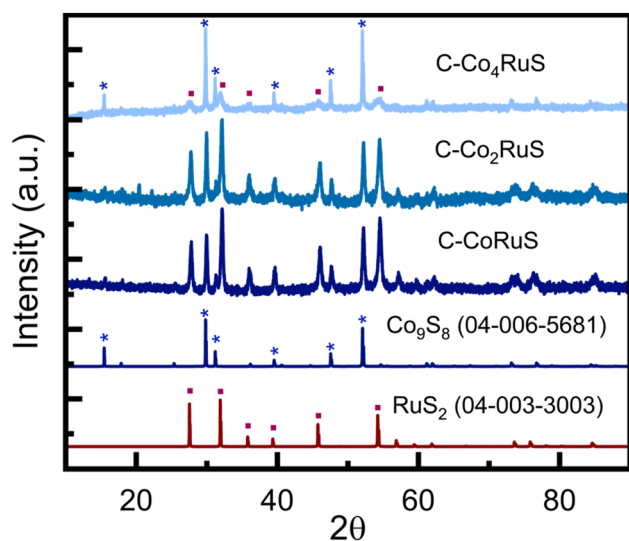


Fig. 1 Powder X-ray diffraction (PXRD) of C-Co_xRuS samples, compared with the standard patterns of RuS₂ (JCPDS No. 04-003-3003, red squares) and Co₉S₈ (JCPDS No. 04-006-5681, blue asterisks), confirms that the characteristic diffraction peaks of both RuS₂ and Co₉S₈ phases are present in all samples.

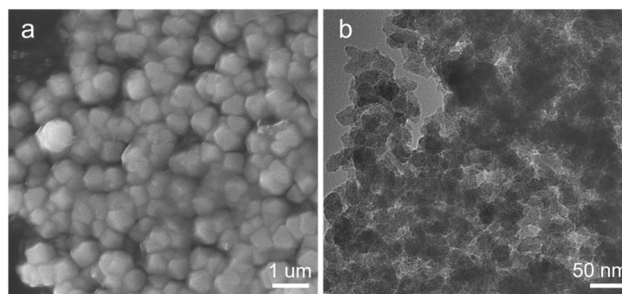


Fig. 2 (a) Scanning electron microscopy (SEM) and (b) Transmission electron microscopy (TEM) images of C-Co₄RuS show polyhedral micron-sized aggregates composed of nanosized particles (5–20 nm).

External morphology appears irregular and non-faceted due to the nature of the solid-state synthesis, which lacks morphology-directing agents. The high thermal energy promotes crystallization, while Vulcan carbon helps disperse and anchor the particles, preventing excessive sintering and supporting nanoscale structuring. This hierarchical architecture can enhance electrochemical performance by providing high accessible active sites and improved electron transport pathways. Furthermore, the energy-dispersion X-ray spectroscopy (EDS) mapping (Fig. S2) confirms that Ru, S, and Co elements are uniformly distributed over the carbon paper electrode.

The surface of the synthesized C-Co₄RuS nanoparticles was analyzed using X-ray photoelectron spectroscopy (XPS). Fig. 3(a)–(d) shows multiple deconvoluted peaks for each element. The deconvoluted Ru 3d spectrum (Fig. 3a) reveals two distinct peaks at 280.2 and 284.6 eV associated with Ru 3d_{5/2} and Ru 3d_{3/2} states, respectively. Further confirmation was obtained from the Ru 3p spectrum (Fig. 3b), which displays sharp peaks at 461.8 and 484.4 eV, assigned to the Ru 3p_{3/2} and Ru 3p_{1/2} states, respectively.⁵⁷ These peaks suggest that the valence state of ruthenium in this sample is +4.^{19,58} In the Co 2p spectrum (Fig. 3c), multiple features observed at 778–785 eV and 793–803 eV are attributed to Co 2p_{3/2} and Co 2p_{1/2}, respectively, along with distinct satellite peaks, which are characteristic of both Co²⁺ and Co³⁺ oxidation states.⁵⁹ This indicates a mixed-valence cobalt environment within the sulfide lattice. The high-resolution S 2p spectrum (Fig. 3d) was deconvoluted into two sulfur doublets corresponding to different sulfur chemical environments. The peaks at lower binding energy are assigned to terminal sulfide species (S²⁻), while the higher-binding-energy doublet is attributed to disulfide species (S₂²⁻) associated with the metal sulfide framework.⁶⁰ Overall, the XPS results confirm the successful incorporation of cobalt and ruthenium into the sulfide framework with mixed oxidation states, which may contribute to enhanced catalytic activity by facilitating redox activity and improved electronic conductivity.

Electrocatalytic performance

The molar ratio of Co : Ru affects the performance of the final electrocatalyst, including the current density, overpotential, and Tafel slope, so ideally, decreasing the amount of ruthenium



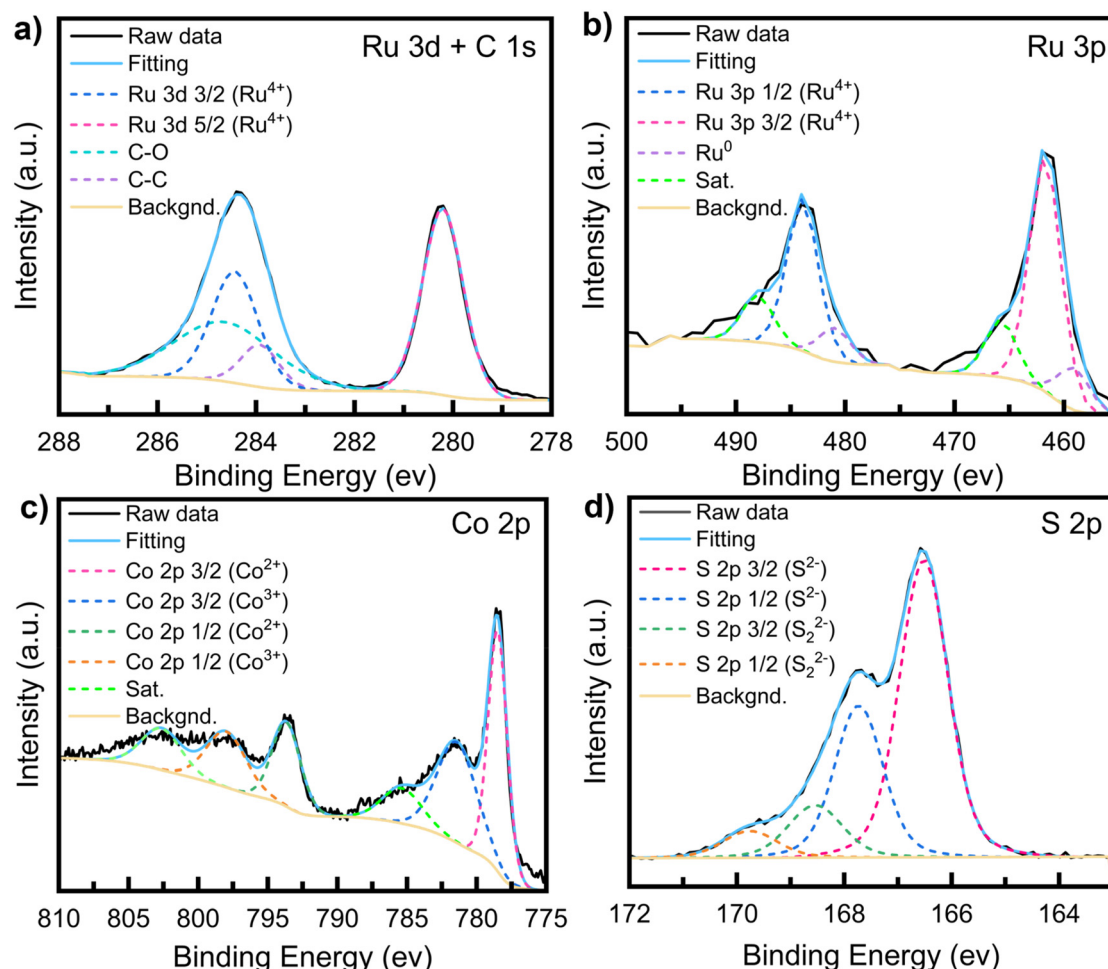


Fig. 3 X-ray photoelectron spectroscopy (XPS) of C-Co₄RuS: (a) Ru 3d and C 1s, (b) Ru 3p, (c) Co 2p, and (d) S 2p binding energy regions. The Co 2p spectrum shows peaks corresponding to Co²⁺ and Co³⁺ oxidation states, while the Ru 3p and Ru 3d spectrum indicates the presence of Ru⁴⁺. The S 2p region was deconvoluted into components attributed to lattice disulfide species (S₂²⁻) and terminal sulfide species (S²⁻). These results confirm the mixed valence states and surface composition characteristic of the bimetallic sulfide catalyst.

nium while maintaining its catalytic behavior is desired. For this purpose, different ratios of Co(NO₃)₂·6H₂O: RuCl₃·xH₂O of 4:1, 2:1, 1:1 and 0:1 were composited with a similar amount of Vulcan carbon in the same flow rate of H₂S. The HER catalytic performance of C-Co_xRuS samples with different Co:Ru ratios and commercial 20% Pt/C was recorded for comparison. The resulting LSV (Linear Sweep Voltammetry) curves were normalized based on the geometrical surface area of the working electrode and were scanned with a scan rate of 5 mV s⁻¹. Fig. 4 shows LSV curves for C-Co_xRuS toward the HER in acidic medium (H₂SO₄ 0.5 M). Cobalt notably boosts the HER activity of ruthenium sulfide, with C-Co₄RuS performing almost as well as the commercial Pt/C catalyst. Also, the overpotential at 10 mA cm⁻² for C-Co₄RuS (-75 mV) is significantly lower than the C-RuS (-194 mV). The Tafel plots in Fig. 5 further explore the HER kinetics of the synthesized catalysts. Commercial 20% Pt/C shows a Tafel slope of 47 mV dec⁻¹, consistent with its well-known catalytic behavior. C-Co₄RuS has a Tafel slope of 75 mV dec⁻¹, indicating significantly enhanced

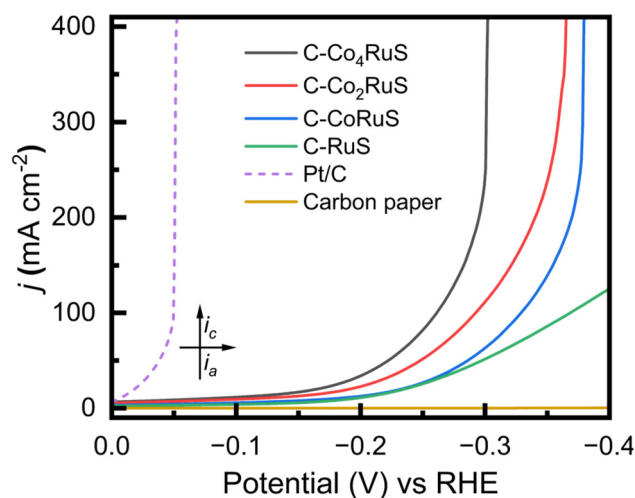


Fig. 4 Linear sweep voltammetry (LSV) curves for C-Co_xRuS catalysts toward the hydrogen evolution reaction (HER) in acidic medium (H₂SO₄ 0.5 M) and scan rate of 5 mV s⁻¹ (as referenced by potential vs. RHE).



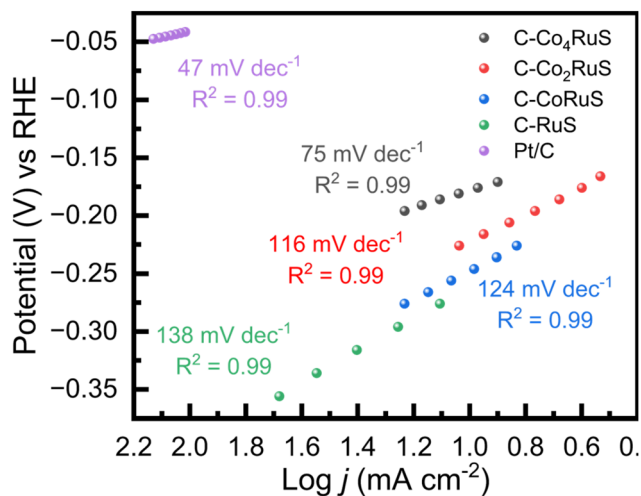


Fig. 5 Tafel plots of C-Co_xRuS for hydrogen evolution reaction (HER) in H₂SO₄ 0.5 M. The Tafel slopes demonstrate that C-Co₄RuS (75 mV dec⁻¹) exhibits significantly enhanced HER kinetics compared to samples with lower cobalt content and approaches the performance of the benchmark Pt/C catalyst (47 mV dec⁻¹).

HER kinetics compared to C-Co₂RuS (116 mV dec⁻¹), C-CoRuS (124 mV dec⁻¹), and C-RuS (138 mV dec⁻¹). This highlights the positive effect of increasing cobalt content on HER kinetics, which suggests that cobalt incorporation improves the kinetics by facilitating faster charge transfer. The Tafel slope can be utilized to characterize the mechanism of HER and its rate-limiting step. In HER, the Volmer step involves the electrochemical adsorption of hydrogen ($H^+ + e^- \rightarrow H^*$), while the Heyrovsky step refers to the electrochemical desorption of hydrogen ($H^* + H^+ + e^- \rightarrow H_2$), and in some systems, two adsorbed hydrogen atoms combine in the Tafel step ($H^* + H^* \rightarrow H_2$).⁶¹ Based on the Tafel slopes, all synthesized samples in this work follow a Volmer–Heyrovsky mechanism, which means they facilitate HER *via* proton adsorption followed by electrochemical desorption, rather than H^{*} recombination.^{62,63}

The polarization curves and Tafel plots in Fig. 6(a–c) compare the oxygen evolution reaction (OER) activity of various catalysts. In Fig. 6a, C-Co₄RuS demonstrates the highest current density and the lowest overpotential among the others, indicating the positive effect of cobalt incorporation on OER performance.

As shown in Fig. 6b, further modification of C-Co₄RuS was made through physical mixture with 10 wt% CoTcPP (CoTcPP/C-Co₄RuS), resulting in enhanced activity compared with pristine C-Co₄RuS and CoTcPP alone, indicating that combining the porphyrin with the sulfide-derived framework provides a beneficial composite effect. The purpose of this combination was to investigate the functional synergy between the molecular Coporphyrin species (which facilitate O–O bond formation *via* Co–N₄ centers) and the conductive C-Co₄RuS framework.

However, while the CoTcPP/Co₄RuS composite has enhanced OER activity, its HER activity was not improved compared to C-Co₄RuS. Yet, the composite catalyst achieves an OER overpotential of 202 mV at 10 mA cm⁻², which is significantly lower than that of CoTcPP (409 mV) and C-Co₄RuS (257 mV), highlighting the improved performance arising from their combination. Also, for further benchmarking, a commercial RuO₂–IrO₂/Ti electrode was evaluated under identical conditions in 1.0 M KOH, showing that the CoTcPP/C-Co₄RuS composite exhibits competitive OER activity while outperforming the parent C-Co₄RuS catalyst. The Tafel plots in Fig. 6c reveal that CoTcPP/C-Co₄RuS exhibits the smallest Tafel slope (79 mV dec⁻¹), lower than C-Co₄RuS (95 mV dec⁻¹) and CoTcPP (163 mV dec⁻¹), indicating faster reaction kinetics and more efficient charge transfer in the composite catalyst. Together, these results highlight the effectiveness of cobalt and porphyrin modification in improving the OER activity of ruthenium sulfide while retaining a relatively low nominal Ru loading (Table S1). Also, as summarized in Table S3, the CoTcPP/C-Co₄RuS catalyst developed in this work delivers an OER overpotential of 202 mV at 10 mA cm⁻² in 1.0 M KOH, which is competitive with several reported Ru-based catalysts in alkaline media. These results suggest that cobalt incorpor-

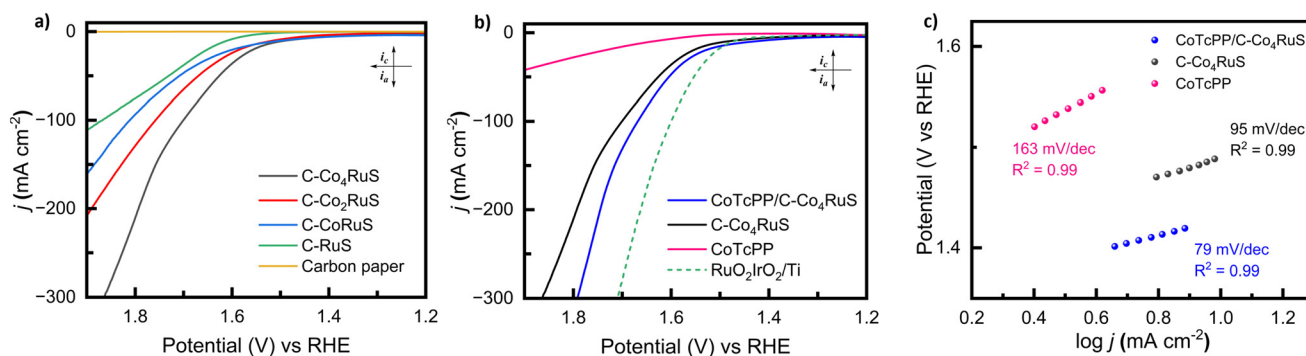


Fig. 6 (a) OER polarization curves of C-Co₄RuS, C-Co₂RuS, C-CoRuS, C-RuS, and carbon paper in KOH 1.0 M, showing enhanced activity with increasing cobalt content. (b) Comparative polarization curves of C-Co₄RuS, CoTcPP, and CoTcPP/C-Co₄RuS catalyst and a commercial RuO₂–IrO₂/Ti benchmark electrode in 1.0 M KOH, demonstrating the improvement in OER performance upon CoTcPP modification. (c) Corresponding OER Tafel plots in KOH 1.0 M, where CoTcPP/C-Co₄RuS exhibits the lowest Tafel slope (79 mV dec⁻¹), confirming faster reaction kinetics compared to individual components.



ation and CoTcPP modification improve the utilization efficiency of ruthenium while maintaining strong OER activity.

To evaluate the overall water splitting performance, the system was tested in a three-electrode configuration using CoTcPP/C-Co₄RuS as the working electrode and C-Co₄RuS as the counter electrode in KOH 1.0 M. As illustrated in Fig. S3, the modified electrode system exhibited improved electrocatalytic behavior, reflected by the increased current response during the measurement. The overpotential required to reach 10 mA cm⁻² was 190 mV, demonstrating that the use of both modified electrodes enhances the overall water-splitting activity.

To better understand the interfacial electron-transfer characteristics of the catalysts, electrochemical impedance spectroscopy (EIS) was carried out in 5 mM [Fe(CN)₆]^{3-/4-} in 0.1 M KCl solution redox probe (at 0.2 V vs. Ag/AgCl), to compare the behavior of the electrodes after each modification step under identical conditions. This measurement was used as a conventional indicator of the relative electron-transfer capability of the electrode surface, rather than as a direct measure of HER or OER kinetics.^{64,65} The results are shown as Nyquist plots in Fig. 7. In these plots, a smaller semicircle in the high-frequency region corresponds to a lower charge-transfer resistance (R_{ct}), indicating more efficient electron transfer toward the redox probe.⁶⁶ The experimental data were fitted using the equivalent circuit model (Fig. S4), and the fitted parameters are summarized in Table S2. As shown in Fig. 7, bare carbon paper exhibits a large semicircle and high R_{ct} (1495 Ω), reflecting relatively poor interfacial electron transfer in the probe electrolyte. Upon introduction of ruthenium and cobalt sulfide, R_{ct} decreased significantly, with C-Co₄RuS showing R_{ct} of 18.1 Ω . The incorporation of CoTcPP further

enhanced the interfacial electron-transfer response, with the CoTcPP/C-Co₄RuS composite displaying the lowest R_{ct} value of 12.79 Ω . This reduction in R_{ct} , along with increased CPE values, suggests improved electronic conductivity. The improved performance of cobalt ruthenium sulfide may be attributed to the combined effect of multivalent cobalt and ruthenium species, which facilitate charge transport within the catalyst framework.

These results align with previous studies on related Ru-Co systems, which have shown that Co incorporation can modify the electronic structure of neighboring Ru sites, enriching the electron density around Ru and suppressing its over-oxidation during catalysis.⁶⁷ Additionally, the conjugated structure of CoTcPP enhances electronic delocalization, further improving charge transport and catalytic activity.

The electrochemically active surface area (ECSA) was estimated using cyclic voltammetry at scan rates of 20, 40, 60, 80, and 100 mV s⁻¹ within the non-faradaic potential region for C-Co₄RuS, CoTcPP, and CoTcPP/C-Co₄RuS composite, as shown in Fig. S5–S7. In this region, where no redox reaction occurs, the measured current is directly proportional to the double-layer capacitance (C_{dl}), which serves as an indicator of the number of accessible electrochemically active sites on the catalyst surface.⁶⁸ The C_{dl} values were extracted from the slopes of the linear fits in plots of the current density difference ($\Delta j = (j_a - j_c)/2$) versus scan rates (Fig. 8). ECSA was then calculated using the relation $ECSA = C_{dl}/C_s$, where C_s is the specific capacitance, typically assumed to be 40 $\mu\text{F cm}^{-2}$ for a smooth surface in 1.0 M KOH. The calculated C_{dl} values were 221.6, 397.2, and 485.1 $\mu\text{F cm}^{-2}$ for CoTcPP, C-Co₄RuS, and CoTcPP/C-Co₄RuS, corresponding to the ECSA values of 5.54, 9.93, and

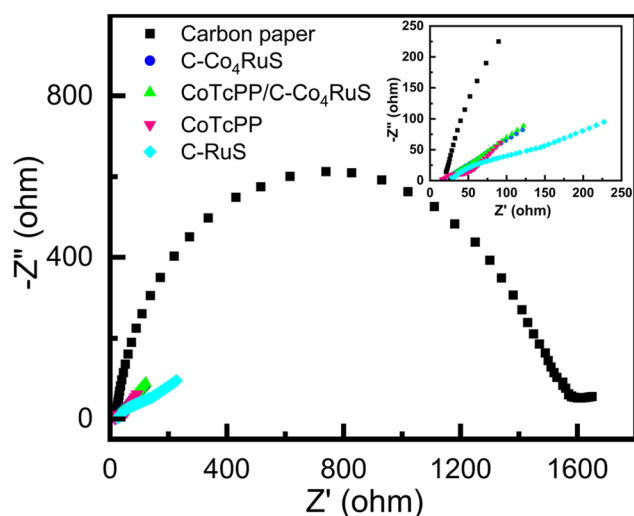


Fig. 7 Nyquist plots of Carbon paper, C-RuS, C-Co₄RuS, CoTcPP, and CoTcPP/C-Co₄RuS obtained from EIS measurements in 5 mM [Fe(CN)₆]^{3-/4-} in 0.1 M KCl solution redox probe (at 0.2 V vs. Ag/AgCl). The smaller semicircle observed for CoTcPP/C-Co₄RuS indicates the lowest charge transfer resistance (R_{ct}) confirming faster interfacial electron transfer compared to the other samples.

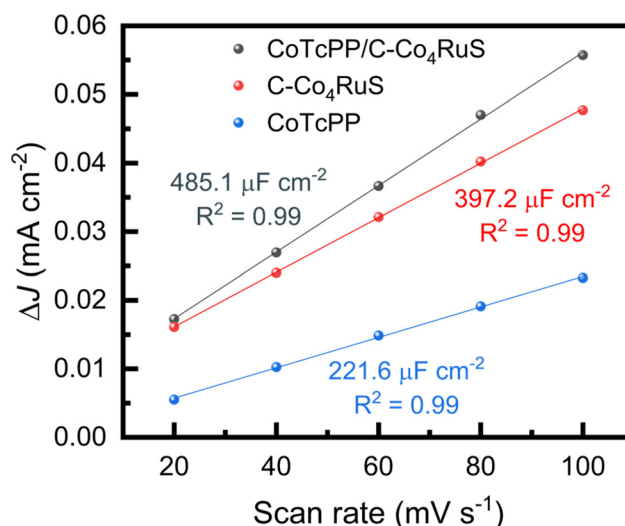


Fig. 8 Plots of current density difference ($\Delta j = (j_a - j_c)/2$) versus scan rate for CoTcPP (blue), C-Co₄RuS (red), and CoTcPP/C-Co₄RuS (gray) measured in the non-faradaic region in 1.0 M KOH. The slopes of the linear fits correspond to the double-layer capacitance (C_{dl}), indicating an increase in electrochemical active surface area (ECSA) upon porphyrin incorporation.



12.13 cm², respectively. The CoTcPP/C-Co₄RuS composite exhibited the highest *C_{dl}* value, indicating the largest electrochemically accessible interfacial area among the samples studied. These results suggest that incorporation of CoTcPP increases the number of exposed catalytic sites, which contributes to enhanced OER performance. Moreover, the ECSA-normalized OER curves (Fig. S8) show that the composite still exhibits higher activity after normalization, indicating that the enhancement can be attributed to interfacial interactions between CoTcPP and C-Co₄RuS.

The ability of a catalyst to maintain its performance during electrochemical reactions is another important factor to consider. For this purpose, the electrochemical stability of the catalyst was tested for 0.1 mg cm⁻² C-Co₄RuS and 0.1 mg cm⁻² CoTcPP/C-Co₄RuS on carbon paper for HER and OER, respectively. The long-term potentiostatic stability tests were carried out at fixed potentials, and the current density was monitored over 20 hours. The applied potentials were chosen slightly beyond the onset potential and near the potential required to achieve 10–15 mA cm⁻², to ensure stable operation in the kinetic regime, minimize transient current fluctuations, and avoid mass-transport limitations (−0.14 V vs. RHE for HER and 1.52 V vs. RHE for OER). As shown in Fig. S9 and S10, the current density is stable during both HER and OER for these time durations. The OER current density of the CoTcPP/C-Co₄RuS composite decreases by only 3% in 25 hours, which can be attributed to the protective and conductive role of the CoTcPP moiety. While the stability of ruthenium sulfide under oxidative conditions is typically limited,⁶⁹ in this work, combining it with CoTcPP significantly improved its durability. The porphyrin likely mitigates surface passivation, preserving the catalytic performance during prolonged OER operation.

To evaluate the surface chemical stability of the catalyst after long-term operation, XPS spectra were collected before and after 25 h of bulk electrolysis in oxidative conditions. As shown in Fig. S11, the characteristic signals of the catalyst are still observed after the durability test, indicating that the main chemical framework is largely preserved. However, minor changes in peak shape and broadening can be seen after electrolysis, suggesting modification of the surface chemical environment during operation. The detected oxygen peak in the electrocatalyst is likely due to the presence of unavoidable oxide species or surface oxidation occurring during exposure to air.⁶¹ Overall, the post-test XPS results indicate that the catalyst maintains its overall composition after 25 h of electrolysis, while undergoing surface evolution that may be associated with the formation of species during catalysis.

Finally, another parameter that can confirm stability is faradaic efficiency (FE). This parameter shows how much of the produced current accounts for hydrogen or oxygen production. A high faradaic efficiency reflects minimal side reactions and excellent selectivity toward the targeted electrochemical process. Faradaic efficiency measurements for HER and OER were conducted in a sealed two-compartment H-cell separated by a Nafion membrane using 1.0 M KOH electrolyte for OER and 0.5 M H₂SO₄ electrolyte for HER. Constant-potential elec-

trolysis was performed at 1.52 V vs. RHE in KOH 1.0 M for OER and −0.14 V vs. RHE in 0.5 M H₂SO₄ for HER for 10 h. The evolved gases were sampled from the headspace using a gas-tight syringe and analyzed by gas chromatography (Shimadzu GC-8A, TCD detector). The faradaic efficiency was calculated according to:

$$FE_{H_2} (\%) = \frac{2Fn_{H_2}}{Q} \times 100 \quad (3)$$

$$FE_{O_2} (\%) = \frac{4Fn_{O_2}}{Q} \times 100 \quad (4)$$

where *F* is Faraday's constant, *n* is the number of measured gas moles, and *Q* is the total charge passed. In this study, the faradaic efficiency for HER was measured to be 96% with C-Co₄RuS, and the CoTcPP/C-Co₄RuS composite had an FE of 95%, for OER confirming that most of the charge passed during electrolysis contributes directly to water splitting, validating the high efficiency and stability of the catalyst.

Overall, electrochemical analyses confirm that combining the multivalent nature of cobalt with ruthenium sulfide enhances both HER and OER performance, while further integration with cobalt porphyrin produces an even more active and durable electrocatalyst for OER. This synergy lowers overpotentials and accelerates reaction kinetics by improving charge-transfer efficiency and increasing active-site accessibility. Stability tests reveal minimal performance loss during prolonged operation, effectively mitigating the oxidative instability typically associated with ruthenium-based catalysts. These results position CoTcPP/C-Co₄RuS as a promising candidate for efficient and scalable water-splitting applications.

Conclusions

In summary, we have developed a one-step, solvent-limited synthetic method to prepare a bimetallic cobalt–ruthenium sulfide electrocatalyst supported on carbon (C-Co₄RuS), as well as its composite with a molecular catalyst, a cobalt-based porphyrin (CoTcPP), for efficient water splitting. The C-Co₄RuS catalyst demonstrates promising HER activity, exhibiting an overpotential of −75 mV at 10 mA cm⁻² and a Tafel slope of 75 mV dec⁻¹ in comparison to C-RuS synthesized through the same method with an overpotential of −194 mV and a Tafel slope of 138 mV dec⁻¹. In the OER experiment, C-Co₄RuS, shows an overpotential of 257 mV at 10 mA cm⁻² with a Tafel slope of 95 mV dec⁻¹. Upon addition of 10% of CoTcPP, the CoTcPP/C-Co₄RuS composite exhibits a reduction of 19% in the overpotential (202 mV) and a 17% improvement in Tafel slope (79 mV dec⁻¹). This improved performance is attributed to the complementary combination between the multivalent metal chalcogenides and the porphyrin units, which facilitates charge transfer, increases the number of active sites, and preserves stability. These findings demonstrate the potential of integrating molecular catalysts with heterogeneous systems to develop efficient water splitting electrocatalysts.



Author contributions

Conceptualization and project administration – Nasim Jafari, Brenda Torres, Dino Villagrán. Methodology, data curation and investigation – Nasim Jafari, Neidy Ocuane, Jose L. Lasso, Brenda Torres. Validation and resources – Dino Villagrán, Brenda Torres, Carlos R. Cabrera. Funding acquisition and supervision – Dino Villagrán. Writing original draft – Nasim Jafari. Review and editing – Nasim Jafari, Neidy Ocuane, Dino Villagrán.

Conflicts of interest

There are no conflicts to declare.

Data availability

The data supporting this article have been included as part of the supplementary information (SI). Supplementary information is available. The Supporting Information includes UV-Vis absorption spectra, EDS elemental mapping and spectra, cyclic voltammograms recorded in the non-Faradaic region, ECSA-normalized OER polarization curves, overall water-splitting and potentiostatic stability measurements, XPS characterization before and after electrolysis, equivalent circuit modeling and fitted EIS parameters, as well as tables summarizing catalyst loading, electrochemical parameters, and comparisons with representative Ru-based electrocatalysts reported in alkaline media. See DOI: <https://doi.org/10.1039/d6qi00499g>.

Acknowledgements

This work was supported by Cleantech (FWP 100898), funded by the U.S. Department of Energy, Office of Science, Basic Energy Sciences, and the Welch Foundation (AH-2083-2024-04-04). We also acknowledge financial support from NSF for the acquisition of the XPS equipment (NSF/CHEM 2216473) and the support of the Center for Alkaline-Based Energy Solutions (CABES), an Energy Frontier Research Center funded by the U. S. Department of Energy (DOE), Office of Science, Basic Energy Sciences (BES), under Award # DE-SC0019445.

References

- S. Chu, Y. Cui and N. Liu, The Path towards Sustainable Energy, *Nat. Mater.*, 2017, **16**(1), 16–22, DOI: [10.1038/nmat4834](https://doi.org/10.1038/nmat4834).
- S.-Y. Bae, J. Mahmood, I.-Y. Jeon and J.-B. Baek, Recent Advances in Ruthenium-Based Electrocatalysts for the Hydrogen Evolution Reaction, *Nanoscale Horiz.*, 2020, **5**(1), 43–56, DOI: [10.1039/C9NH00485H](https://doi.org/10.1039/C9NH00485H).
- F. Dawood, M. Anda and G. M. Shafiullah, Hydrogen Production for Energy: An Overview, *Int. J. Hydrogen Energy*, 2020, **45**(7), 3847–3869, DOI: [10.1016/j.ijhydene.2019.12.059](https://doi.org/10.1016/j.ijhydene.2019.12.059).
- M. Dehghanimadvar, R. Shirmohammadi, M. Sadeghzadeh, A. Aslani and R. Ghasempour, Hydrogen Production Technologies: Attractiveness and Future Perspective, *Int. J. Energy Res.*, 2020, **44**(11), 8233–8254, DOI: [10.1002/er.5508](https://doi.org/10.1002/er.5508).
- S. O. Jeje, T. Marazani, J. O. Obiko and M. B. Shongwe, Advancing the Hydrogen Production Economy: A Comprehensive Review of Technologies, Sustainability, and Future Prospects, *Int. J. Hydrogen Energy*, 2024, **78**, 642–661, DOI: [10.1016/j.ijhydene.2024.06.344](https://doi.org/10.1016/j.ijhydene.2024.06.344).
- J. Wang, F. Xu, H. Jin, Y. Chen and Y. Wang, Non-Noble Metal-based Carbon Composites in Hydrogen Evolution Reaction: Fundamentals to Applications, *Adv. Mater.*, 2017, **29**(14), 1605838, DOI: [10.1002/adma.201605838](https://doi.org/10.1002/adma.201605838).
- A. Raveendran, M. Chandran and R. Dhanusuraman, A Comprehensive Review on the Electrochemical Parameters and Recent Material Development of Electrochemical Water Splitting Electrocatalysts, *RSC Adv.*, 2023, **13**(6), 3843–3876, DOI: [10.1039/D2RA07642J](https://doi.org/10.1039/D2RA07642J).
- J. Ying, J.-B. Chen, Y.-X. Xiao, S. I. Cordoba De Torresi, K. I. Ozoemena and X.-Y. Yang, Recent Advances in Ru-Based Electrocatalysts for Oxygen Evolution Reaction, *J. Mater. Chem. A*, 2023, **11**(4), 1634–1650, DOI: [10.1039/D2TA07196G](https://doi.org/10.1039/D2TA07196G).
- S. Nishioka, F. E. Osterloh, X. Wang, T. E. Mallouk and K. Maeda, Photocatalytic Water Splitting, *Nat. Rev. Methods Primers*, 2023, **3**(1), 42, DOI: [10.1038/s43586-023-00226-x](https://doi.org/10.1038/s43586-023-00226-x).
- W. Li, H. Tian, L. Ma, Y. Wang, X. Liu and X. Gao, Low-Temperature Water Electrolysis: Fundamentals, Progress, and New Strategies, *Mater. Adv.*, 2022, **3**(14), 5598–5644, DOI: [10.1039/D2MA00185C](https://doi.org/10.1039/D2MA00185C).
- L. Fei, H. Sun, Y. Li, Y. Gu, W. Zhou and Z. Shao, Recent Advances in Innovative Systems for Electrocatalytic Hydrogen Production, *Energy Environ. Sci.*, 2025, **18**(13), 6456–6529, DOI: [10.1039/D4EE03084B](https://doi.org/10.1039/D4EE03084B).
- Y. Yu, G. Li, Y. Xiao, C. Chen, Y. Bai, T. Wang, J. Li, Y. Hua, D. Wu, P. Rao, P. Deng, X. Tian and Y. Yuan, Iridium-Based Electrocatalysts for Acidic Oxygen Evolution Reaction, *J. Energy Chem.*, 2025, **103**, 200–224, DOI: [10.1016/j.jechem.2024.11.033](https://doi.org/10.1016/j.jechem.2024.11.033).
- C. Wu, Y. Yu, Y. Song, P. Rao, X. Han, Y. Liang, J. Li, K. Zhang, Z. Zhang, P. Deng, X. Tian and D. Wu, Pyrrole-Type TM-N3 Sites as High-Efficient Bifunctional Oxygen Reactions Electrocatalysts: From Theoretical Prediction to Experimental Validation, *J. Energy Chem.*, 2025, **104**, 472–481, DOI: [10.1016/j.jechem.2025.01.002](https://doi.org/10.1016/j.jechem.2025.01.002).
- M. A. Qadeer, X. Zhang, M. A. Farid, M. Tanveer, Y. Yan, S. Du, Z.-F. Huang, M. Tahir and J.-J. Zou, A Review on Fundamentals for Designing Hydrogen Evolution Electrocatalyst, *J. Power Sources*, 2024, **613**, 234856, DOI: [10.1016/j.jpowsour.2024.234856](https://doi.org/10.1016/j.jpowsour.2024.234856).
- N. Cheng, S. Stambula, D. Wang, M. N. Banis, J. Liu, A. Riese, B. Xiao, R. Li, T.-K. Sham, L.-M. Liu, G. A. Botton and X. Sun, Platinum Single-Atom and Cluster Catalysis of



- the Hydrogen Evolution Reaction, *Nat. Commun.*, 2016, 7(1), 13638, DOI: [10.1038/ncomms13638](https://doi.org/10.1038/ncomms13638).
- 16 R. Subbaraman, D. Tripkovic, D. Strmcnik, K.-C. Chang, M. Uchimura, A. P. Paulikas, V. Stamenkovic and N. M. Markovic, Enhancing Hydrogen Evolution Activity in Water Splitting by Tailoring $\text{Li}^+ \text{-Ni(OH)}_2 \text{-Pt}$ Interfaces, *Science*, 2011, 334(6060), 1256–1260, DOI: [10.1126/science.1211934](https://doi.org/10.1126/science.1211934).
- 17 J. N. Tiwari, S. Sultan, C. W. Myung, T. Yoon, N. Li, M. Ha, A. M. Harzandi, H. J. Park, D. Y. Kim, S. S. Chandrasekaran, W. G. Lee, V. Vij, H. Kang, T. J. Shin, H. S. Shin, G. Lee, Z. Lee and K. S. Kim, Multicomponent Electrocatalyst with Ultralow Pt Loading and High Hydrogen Evolution Activity, *Nat. Energy*, 2018, 3(9), 773–782, DOI: [10.1038/s41560-018-0209-x](https://doi.org/10.1038/s41560-018-0209-x).
- 18 M. Smiljanić, S. Panić, M. Bele, F. Ruiz-Zepeda, L. Pavko, L. Gašparič, A. Kokalj, M. Gaberšček and N. Hodnik, Improving the HER Activity and Stability of Pt Nanoparticles by Titanium Oxynitride Support, *ACS Catal.*, 2022, 12(20), 13021–13033, DOI: [10.1021/acscatal.2c03214](https://doi.org/10.1021/acscatal.2c03214).
- 19 P. Li, X. Duan, S. Wang, L. Zheng, Y. Li, H. Duan, Y. Kuang and X. Sun, Amorphous Ruthenium–Sulfide with Isolated Catalytic Sites for Pt–Like Electrocatalytic Hydrogen Production Over Whole pH Range, *Small*, 2019, 15(46), 1904043, DOI: [10.1002/smll.201904043](https://doi.org/10.1002/smll.201904043).
- 20 S. Sahoo, P. Pazhamalai, K. Krishnamoorthy and S.-J. Kim, Hydrothermally Prepared $\alpha\text{-MnSe}$ Nanoparticles as a New Pseudocapacitive Electrode Material for Supercapacitor, *Electrochim. Acta*, 2018, 268, 403–410, DOI: [10.1016/j.electacta.2018.02.116](https://doi.org/10.1016/j.electacta.2018.02.116).
- 21 V. Raman, D. Chinnadurai, R. Rajmohan, V. T. Chebrolu, V. Rajangam and H.-J. Kim, Transition Metal Chalcogenide Based MnSe Heterostructured with NiCo_2O_4 as a New High Performance Electrode Material for Capacitive Energy Storage, *New J. Chem.*, 2019, 43(32), 12630–12640, DOI: [10.1039/C9NJ02711D](https://doi.org/10.1039/C9NJ02711D).
- 22 Y. Ge, Y. Wu, L. Ma, X. Li, M. Román, R. R. Chianelli, B. Torres and D. Villagrán, Amine and Carbon-Pretreated Nickel–Molybdenum Disulfide as Bifunctional Electrocatalysts for Hydrogen and Oxygen Gas Evolution, *Int. J. Hydrogen Energy*, 2022, 47(65), 27839–27847, DOI: [10.1016/j.ijhydene.2022.06.114](https://doi.org/10.1016/j.ijhydene.2022.06.114).
- 23 S. Feng, P. Rao, X. Wu, K. Li, A. Qi, Y. Yu, J. Li, P. Deng, Y. Yuan, S. Wang, X. Tian and Z. Kang, *In-situ* Generation of Hydroxyl Layers in $\text{CoO} @ \text{FeSe}_2$ Catalyst for High Selectivity Seawater Electrolysis, *Chin. J. Chem.*, 2024, 42(1), 48–54, DOI: [10.1002/cjoc.202300441](https://doi.org/10.1002/cjoc.202300441).
- 24 J. Yu, Y. Guo, S. Miao, M. Ni, W. Zhou and Z. Shao, Spherical Ruthenium Disulfide-Sulfur-Doped Graphene Composite as an Efficient Hydrogen Evolution Electrocatalyst, *ACS Appl. Mater. Interfaces*, 2018, 10(40), 34098–34107, DOI: [10.1021/acsami.8b08239](https://doi.org/10.1021/acsami.8b08239).
- 25 S. Shima, O. Pilak, S. Vogt, M. Schick, M. S. Stagni, W. Meyer-Klaucke, E. Warkentin, R. K. Thauer and U. Ermler, The Crystal Structure of [Fe]-Hydrogenase Reveals the Geometry of the Active Site, *Science*, 2008, 321(5888), 572–575, DOI: [10.1126/science.1158978](https://doi.org/10.1126/science.1158978).
- 26 D.-Y. Wang, M. Gong, H.-L. Chou, C.-J. Pan, H.-A. Chen, Y. Wu, M.-C. Lin, M. Guan, J. Yang, C.-W. Chen, Y.-L. Wang, B.-J. Hwang, C.-C. Chen and H. Dai, Highly Active and Stable Hybrid Catalyst of Cobalt-Doped FeS_2 Nanosheets–Carbon Nanotubes for Hydrogen Evolution Reaction, *J. Am. Chem. Soc.*, 2015, 137(4), 1587–1592, DOI: [10.1021/ja511572q](https://doi.org/10.1021/ja511572q).
- 27 Y. Kuo, Hydrogenation and Hydrodesulfurization over Sulfided Ruthenium Catalysts II. Impact of Surface Phase Behavior on Activity and Selectivity, *J. Catal.*, 1988, 112(1), 250–266, DOI: [10.1016/0021-9517\(88\)90138-8](https://doi.org/10.1016/0021-9517(88)90138-8).
- 28 E. J. Popczun, J. R. McKone, C. G. Read, A. J. Biacchi, A. M. Wiltrout, N. S. Lewis and R. E. Schaak, Nanostructured Nickel Phosphide as an Electrocatalyst for the Hydrogen Evolution Reaction, *J. Am. Chem. Soc.*, 2013, 135(25), 9267–9270, DOI: [10.1021/ja403440e](https://doi.org/10.1021/ja403440e).
- 29 Y. Yang, Y. Yu, J. Li, Q. Chen, Y. Du, P. Rao, R. Li, C. Jia, Z. Kang, P. Deng, Y. Shen and X. Tian, Engineering Ruthenium-Based Electrocatalysts for Effective Hydrogen Evolution Reaction, *Nano-Micro Lett.*, 2021, 13(1), 160, DOI: [10.1007/s40820-021-00679-3](https://doi.org/10.1007/s40820-021-00679-3).
- 30 M. Smiljanić, M. Bele, L. Pavko, A. Hrnjić, F. Ruiz-Zepeda, L. Bijelić, A. R. Kamšek, M. Nuhanović, A. Marsel, L. Gašparič, A. Kokalj and N. Hodnik, Titanium Oxynitride-Supported Ru Nanoparticles as Exceptional Electrocatalysts for Alkaline Hydrogen Evolution Reaction, *Chem. Eng. J.*, 2025, 517, 164204, DOI: [10.1016/j.cej.2025.164204](https://doi.org/10.1016/j.cej.2025.164204).
- 31 Z. Liu, S. Zhao, B. Liu, P. Wang and T. Yi, Multidimensional Design of Carbon-Supported Ru-Based Catalysts: A Journey to Hydrogen Evolution Reaction Performance Breakthroughs, *Chem. Sci.*, 2026, 17(1), 52–95, DOI: [10.1039/D5SC06468F](https://doi.org/10.1039/D5SC06468F).
- 32 S. M. El-Refaei, P. A. Russo, T. Schultz, Z. Chen, P. Amsalem, N. Koch and N. Pinna, Activating Ru in the Pyramidal Sites of Ru_2 P-type Structures with Earth-abundant Transition Metals for Achieving Extremely High HER Activity While Minimizing Noble Metal Content, *Carbon Energy*, 2024, 6(9), e556, DOI: [10.1002/cey2.556](https://doi.org/10.1002/cey2.556).
- 33 Y. Xu, C. Du, Q. Shen, J. Huang, X. Zhang and J. Chen, Well-Dispersed Pyrite-Type RuS_2 Nanocrystals Anchored on Porous Nitrogen and Sulfur Co-Doped Hollow Carbon Spheres for Enhanced Alkaline Hydrogen Evolution, *Chem. Eng. J.*, 2021, 417, 129318, DOI: [10.1016/j.cej.2021.129318](https://doi.org/10.1016/j.cej.2021.129318).
- 34 T. Su, B. Guan, J. Zhou, C. Zheng, J. Guo, J. Chen, Y. Zhang, Y. Yuan, W. Xie, N. Zhou, H. Dang, B. Xu and Z. Huang, Review on Ru-Based and Ni-Based Catalysts for Ammonia Decomposition: Research Status, Reaction Mechanism, and Perspectives, *Energy Fuels*, 2023, 37(12), 8099–8127, DOI: [10.1021/acs.energyfuels.3c00804](https://doi.org/10.1021/acs.energyfuels.3c00804).
- 35 H. Zhu, J. Zhang, R. Yanzhang, M. Du, Q. Wang, G. Gao, J. Wu, G. Wu, M. Zhang, B. Liu, J. Yao and X. Zhang, When Cubic Cobalt Sulfide Meets Layered Molybdenum Disulfide: A Core–Shell System Toward Synergetic Electrocatalytic Water Splitting, *Adv. Mater.*, 2015, 27(32), 4752–4759, DOI: [10.1002/adma.201501969](https://doi.org/10.1002/adma.201501969).



- 36 H. Zhao, J. Wu, T. Chen, P. Yan, W. Yao, X. Ma, Y. Sun, W. Wang and M. Shi, Cobalt-Doped Molybdenum Sulfide as an Interlayer Facilitates Polysulfide Conversion to Obtain High-Performance Lithium–sulfur Batteries, *J. Energy Storage*, 2024, **101**, 113903, DOI: [10.1016/j.est.2024.113903](https://doi.org/10.1016/j.est.2024.113903).
- 37 R. Bolagam and S. Um, Hydrothermal Synthesis of Cobalt Ruthenium Sulfides as Promising Pseudocapacitor Electrode Materials, *Coatings*, 2020, **10**(3), 200, DOI: [10.3390/coatings10030200](https://doi.org/10.3390/coatings10030200).
- 38 I. Barraza Alvarez, Y. Wu, J. Sanchez, Y. Ge, M. V. Ramos-Garcés, T. Chu, T. F. Jaramillo, J. L. Colón and D. Villagrán, Cobalt Porphyrin Intercalation into Zirconium Phosphate Layers for Electrochemical Water Oxidation, *Sustainable Energy Fuels*, 2021, **5**(2), 430–437, DOI: [10.1039/D0SE01134G](https://doi.org/10.1039/D0SE01134G).
- 39 N. Ocuane, B. A. Dorsey, S. P. Suman, M. Ramírez Ramos, H. Banda and D. Villagrán, Interface Anchoring of Cobalt Porphyrin on a Conductive Metal Organic Framework Platform for Water Electrolysis, *ACS Appl. Mater. Interfaces*, 2025, **18**(1), 1312–1323, DOI: [10.1021/acsami.5c19333](https://doi.org/10.1021/acsami.5c19333), acsami.5c19333.
- 40 X. Li, H. Lei, L. Xie, N. Wang, W. Zhang and R. Cao, Metalloporphyrins as Catalytic Models for Studying Hydrogen and Oxygen Evolution and Oxygen Reduction Reactions, *Acc. Chem. Res.*, 2022, **55**(6), 878–892, DOI: [10.1021/acs.accounts.1c00753](https://doi.org/10.1021/acs.accounts.1c00753).
- 41 Z. Liang, H.-Y. Wang, H. Zheng, W. Zhang and R. Cao, Porphyrin-Based Frameworks for Oxygen Electrocatalysis and Catalytic Reduction of Carbon Dioxide, *Chem. Soc. Rev.*, 2021, **50**(4), 2540–2581, DOI: [10.1039/D0CS01482F](https://doi.org/10.1039/D0CS01482F).
- 42 Y. Ge, Z. Lyu, M. Marcos-Hernández and D. Villagrán, Free-Base Porphyrin Polymer for Bifunctional Electrochemical Water Splitting, *Chem. Sci.*, 2022, **13**(29), 8597–8604, DOI: [10.1039/D2SC01250B](https://doi.org/10.1039/D2SC01250B).
- 43 N. Ocuane, N. Jafari, J. J. Calvillo Solis, M. Saucedo and D. Villagrán, Porphyrin-Functionalized Glassy Carbon Electrodes for Electrochemical Water Splitting, *Dalton Trans.*, 2025, **54**(33), 12550–12556, DOI: [10.1039/D5DT01390A](https://doi.org/10.1039/D5DT01390A).
- 44 N. Ocuane, Y. Ge, C. Sandoval-Pauker and D. Villagrán, Bifunctional Porphyrin-Based Metal–Organic Polymers for Electrochemical Water Splitting, *Dalton Trans.*, 2024, **53**(5), 2306–2317, DOI: [10.1039/D3DT03371F](https://doi.org/10.1039/D3DT03371F).
- 45 M. Joseph and S. Haridas, Recent Progresses in Porphyrin Assisted Hydrogen Evolution, *Int. J. Hydrogen Energy*, 2020, **45**(21), 11954–11975, DOI: [10.1016/j.ijhydene.2020.02.103](https://doi.org/10.1016/j.ijhydene.2020.02.103).
- 46 Z. Liang, G. Zhou, H. Tan, Y. Mou, J. Zhang, H. Guo, S. Yang, H. Lei, H. Zheng, W. Zhang, H. Lin and R. Cao, Constructing Co₄ (SO₄)₄ Clusters within Metal–Organic Frameworks for Efficient Oxygen Electrocatalysis, *Adv. Mater.*, 2024, **36**(38), 2408094, DOI: [10.1002/adma.202408094](https://doi.org/10.1002/adma.202408094).
- 47 X. Peng, J. Han, X. Li, G. Liu, Y. Xu, Y. Peng, S. Nie, W. Li, X. Li, Z. Chen, H. Peng, R. Cao and Y. Fang, Electrocatalytic Hydrogen Evolution with a Copper Porphyrin Bearing Meso-(o-Carborane) Substituents, *Chem. Commun.*, 2023, **59**(72), 10777–10780, DOI: [10.1039/D3CC03104G](https://doi.org/10.1039/D3CC03104G).
- 48 X. Peng, M. Zhang, H. Qin, J. Han, Y. Xu, W. Li, X. Zhang, W. Zhang, U. Apfel and R. Cao, Switching Electrocatalytic Hydrogen Evolution Pathways through Electronic Tuning of Copper Porphyrins, *Angew. Chem.*, 2024, **136**(13), e202401074, DOI: [10.1002/ange.202401074](https://doi.org/10.1002/ange.202401074).
- 49 D. Li, C. Lin, C. Batchelor-McAuley, L. Chen and R. G. Compton, Tafel Analysis in Practice, *J. Electroanal. Chem.*, 2018, **826**, 117–124, DOI: [10.1016/j.jelechem.2018.08.018](https://doi.org/10.1016/j.jelechem.2018.08.018).
- 50 C. Wei, S. Sun, D. Mandler, X. Wang, S. Z. Qiao and Z. J. Xu, Approaches for Measuring the Surface Areas of Metal Oxide Electrocatalysts for Determining Their Intrinsic Electrocatalytic Activity, *Chem. Soc. Rev.*, 2019, **48**(9), 2518–2534, DOI: [10.1039/C8CS00848E](https://doi.org/10.1039/C8CS00848E).
- 51 A. J. Bard, L. R. Faulkner and H. S. White, *Electrochemical Methods: Fundamentals and Applications*, John Wiley & Sons, 2022.
- 52 P. H. Edwards, J. R. Bairan Espano and J. E. Macdonald, Rational Phase Control in the Synthesis of Cobalt Sulfides, *Chem. Mater.*, 2024, **36**(15), 7186–7196, DOI: [10.1021/acs.chemmater.4c00911](https://doi.org/10.1021/acs.chemmater.4c00911).
- 53 Q. R. Hu, S. L. Wang, Y. Zhang and W. H. Tang, Synthesis of Cobalt Sulfide Nanostructures by a Facile Solvothermal Growth Process, *J. Alloys Compd.*, 2010, **491**(1–2), 707–711, DOI: [10.1016/j.jallcom.2009.11.050](https://doi.org/10.1016/j.jallcom.2009.11.050).
- 54 J. A. Aliaga, J. F. Araya, H. Lozano, E. Benavente, G. Alonso-Núñez and G. González, An Easy One-Pot Solvothermal Synthesis of Poorly Crystalline Solid ReS₂/C Microspheres, *Mater. Chem. Phys.*, 2015, **151**, 372–377, DOI: [10.1016/j.matchemphys.2014.12.012](https://doi.org/10.1016/j.matchemphys.2014.12.012).
- 55 A. Balakrishnan, J. D. Groeneveld, S. Pokhrel and L. Mädler, Metal Sulfide Nanoparticles: Precursor Chemistry, *Chem. – Eur. J.*, 2021, **27**(21), 6390–6406, DOI: [10.1002/chem.202004952](https://doi.org/10.1002/chem.202004952).
- 56 R. Zhuang, J. Yang and J. Wu, Co₉S₈@CNFs Cathode Enables Stable Aluminum Storage with 3D Synergy and Co-Dominated Mechanism, *Electrochem. Commun.*, 2025, **177**, 107989, DOI: [10.1016/j.elecom.2025.107989](https://doi.org/10.1016/j.elecom.2025.107989).
- 57 K. Krishnamoorthy, P. Pazhamalai and S. J. Kim, Ruthenium Sulfide Nanoparticles as a New Pseudocapacitive Material for Supercapacitor, *Electrochim. Acta*, 2017, **227**, 85–94, DOI: [10.1016/j.electacta.2016.12.171](https://doi.org/10.1016/j.electacta.2016.12.171).
- 58 D. J. Morgan, Resolving Ruthenium: XPS Studies of Common Ruthenium Materials, *Surf. Interface Anal.*, 2015, **47**(11), 1072–1079, DOI: [10.1002/sia.5852](https://doi.org/10.1002/sia.5852).
- 59 H. Liu, Z. You, S. Yang, C. Liu, X. Xie, K. Xiang, X. Wang and X. Yan, High-Efficient Adsorption and Removal of Elemental Mercury from Smelting Flue Gas by Cobalt Sulfide, *Environ. Sci. Pollut. Res.*, 2019, **26**(7), 6735–6744, DOI: [10.1007/s11356-019-04159-5](https://doi.org/10.1007/s11356-019-04159-5).
- 60 M.-R. Gao, J.-X. Liang, Y.-R. Zheng, Y.-F. Xu, J. Jiang, Q. Gao, J. Li and S.-H. Yu, An Efficient Molybdenum Disulfide/Cobalt Diselenide Hybrid Catalyst for



- Electrochemical Hydrogen Generation, *Nat. Commun.*, 2015, **6**(1), 5982, DOI: [10.1038/ncomms6982](https://doi.org/10.1038/ncomms6982).
- 61 M. Sadangi and J. N. Behera, Ruthenium-Doped Cobalt Sulphide Electrocatalyst Derived from a Ruthenium–Cobalt Prussian Blue Analogue (RuCo-PBA) for an Enhanced Hydrogen Evolution Reaction (HER), *Dalton Trans.*, 2024, **53**(15), 6667–6675, DOI: [10.1039/D4DT00099D](https://doi.org/10.1039/D4DT00099D).
- 62 D. S. P. Cardoso, S. Eugénio, T. M. Silva, D. M. F. Santos, C. A. C. Sequeira and M. F. Montemor, Hydrogen Evolution on Nanostructured Ni–Cu Foams, *RSC Adv.*, 2015, **5**(54), 43456–43461, DOI: [10.1039/C5RA06517H](https://doi.org/10.1039/C5RA06517H).
- 63 T. Shinagawa, A. T. Garcia-Esparza and K. Takanebe, Insight on Tafel Slopes from a Microkinetic Analysis of Aqueous Electrocatalysis for Energy Conversion, *Sci. Rep.*, 2015, **5**(1), 13801, DOI: [10.1038/srep13801](https://doi.org/10.1038/srep13801).
- 64 A. Adiraju, A. Jalasutram, A. Al-Hamry, M. Talbi, J. Wang, C. Tegenkamp and O. Kanoun, Laser-Induced Fibers and Copper Phthalocyanine Modified Laser-Induced Graphene Electrodes for Sensitive and Selective Electrochemical Detection of Nitrite, *RSC Adv.*, 2024, **14**(39), 28648–28658, DOI: [10.1039/D4RA03341H](https://doi.org/10.1039/D4RA03341H).
- 65 S. Vogt, Q. Su, C. Gutiérrez-Sánchez and G. Nöll, Critical View on Electrochemical Impedance Spectroscopy Using the Ferri/Ferrocyanide Redox Couple at Gold Electrodes, *Anal. Chem.*, 2016, **88**(8), 4383–4390, DOI: [10.1021/acs.analchem.5b04814](https://doi.org/10.1021/acs.analchem.5b04814).
- 66 N. O. Laschuk, E. B. Easton and O. V. Zenkina, Reducing the Resistance for the Use of Electrochemical Impedance Spectroscopy Analysis in Materials Chemistry, *RSC Adv.*, 2021, **11**(45), 27925–27936, DOI: [10.1039/D1RA03785D](https://doi.org/10.1039/D1RA03785D).
- 67 K. Shah, R. Dai, M. Mateen, Z. Hassan, Z. Zhuang, C. Liu, M. Israr, W. Cheong, B. Hu, R. Tu, C. Zhang, X. Chen, Q. Peng, C. Chen and Y. Li, Cobalt Single Atom Incorporated in Ruthenium Oxide Sphere: A Robust Bifunctional Electrocatalyst for HER and OER, *Angew. Chem., Int. Ed.*, 2022, **61**(4), e202114951, DOI: [10.1002/anie.202114951](https://doi.org/10.1002/anie.202114951).
- 68 A. Karmakar and S. Kundu, A Concise Perspective on the Effect of Interpreting the Double Layer Capacitance Data over the Intrinsic Evaluation Parameters in Oxygen Evolution Reaction, *Mater. Today Energy*, 2023, **33**, 101259, DOI: [10.1016/j.mtener.2023.101259](https://doi.org/10.1016/j.mtener.2023.101259).
- 69 C. Ling, H.-B. Li, C.-Z. Yuan, Z. Yang, H.-B. Chong, X.-J. Qian, X.-J. Lu, T.-Y. Cheang and A.-W. Xu, Sulfur Doped Ruthenium Nanoparticles as a Highly Efficient Electrocatalyst for the Hydrogen Evolution Reaction in Alkaline Media, *Catal. Sci. Technol.*, 2021, **11**(11), 3865–3872, DOI: [10.1039/D1CY00621E](https://doi.org/10.1039/D1CY00621E).

